



QUANTUM INTERNET ALLIANCE



D2.2 Report on highly multimode memories

Document History

Revision Nr	Description	Author	Review	Date
1	First draft	Afzelius/de Riedmatten/Tittel/Laurat		10.03.2021
2	Revised version	Afzelius/de Riedmatten/Tittel/Laurat		22.03.2021

This project has received funding from the European Union's Horizon 2020 research and innovation programme under grant agreement No 820445.

The opinions expressed in this document reflect only the author's view and in no way reflect the European Commission's opinions. The European Commission is not responsible for any use that may be made of the information it contains.

Index

1. Abstract	5
2. Keyword list	5
3. Acronyms & Abbreviations	5
4. Introduction	6
5. Time and frequency multiplexed solid-state quantum memory with fixed storage time	7
5.1. Time multiplexing in Europium doped Y_2SiO_5 (UNIGE)	7
5.2. Time and frequency multiplexing in Praseodymium doped Y_2SiO_5 (ICFO)	8
5.3. Frequency and time multiplexing in $Tm:Y_3Ga_5O_{12}$ (TUD)	10
6. Time multiplexing in solid-state quantum memories with on-demand read out	12
7. Space-division multiplexing in cold-atom-based quantum memories	14
8. Conclusion	17
9. References	18

1. Abstract

In this report we describe the progress made in QIA regarding multiplexing of ensemble-based quantum memories for quantum repeaters. Multiplexing capacity is a key parameter for quantum repeaters, as the long-distance entanglement distribution rate is directly proportional to the capacity. We report that partners within WP2 have demonstrated multimode capacities beyond 100 modes using time and frequency multiplexing, or combination of both, in rare-earth-doped crystals and that first steps have been taken to demonstrate spatial division multiplexing in cold atomic vapors.

2. Keyword list

Ensemble-based quantum memories, temporal multiplexing, frequency multiplexing, spatial multiplexing

3. Acronyms & Abbreviations

DoA	Description of Action
EC	European Commission
WP	Work Package
AFC	Atomic frequency comb
SW	Spin wave

4. Introduction

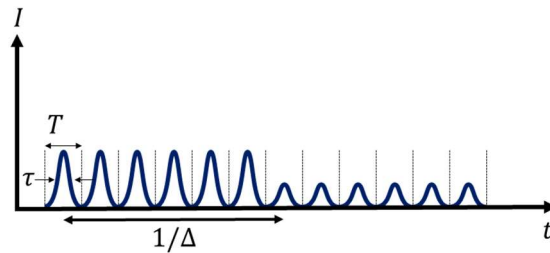
WP2 will develop the required technologies for quantum repeaters (QRs). A key requirement for quantum repeaters based on heralded entanglement is the need for massive multiplexing (see Approach 1 and 2 as described in the project application). The main challenge in multiplexing a quantum repeater lies in developing quantum memories (QMs) that can store a large number of modes, using time, frequency or spatial degrees freedom (or a combination of these). This report will describe the progress made in QIA with respect to multimode quantum memories, which is the objective of Task 2.2: “Multiplexing Quantum Nodes” in WP2. We recall that within WP2 we investigate two physical systems for heralded entanglement QRs; rare-earth-doped crystals and laser-cooled alkali atoms.

Rare-earth doped crystals are excellent candidates for scalable and highly multimode quantum memories. Frequency multiplexing can be easily exploited by engineering the inhomogeneously broadened transitions of rare-earth ions. Moreover, we can take advantage of the intrinsic temporal multimodality of the atomic frequency comb protocol. Finally, thanks to their solid-state nature, high spatial multimodality can be accessed in an integrated fashion, e.g. with the fabrication of matrices of waveguides.

Thanks to their demonstrated high efficiency and long storage times, other excellent candidates for quantum nodes are laser-cooled alkali atoms. A challenge with these systems is multiplexing, as frequency multiplexing is impossible and time multiplexing requires an active control of the spin inhomogeneous broadening. However, it has been shown recently that multiplexing is possible through spatial multimode storage. In WP2 we investigate spatial multimode storage based on Hermite Gaussian (HG) modes, inspired by recent progress in classical fibre communication technologies.

5. Time and frequency multiplexed solid-state quantum memory with fixed storage time

The atomic frequency comb (AFC) quantum memory can be operated with a fixed storage time by storing the input states as optical excitations. The storage time is then the inverse of the periodicity of the AFC structure, $1/\Delta$. The AFC memory is ideally suited for multimode temporal storage (**temporal multiplexing**), as a train of optical input pulses can be stored, as illustrated



below:

Here a temporal mode has a total duration of T , and the intensity FWHM of the input mode is denoted by τ . In addition one can **multiplex in frequency space**, by creating multiple AFCs within the large optical inhomogeneous broadening, where each AFC can have different fixed storage times. This section will describe the progress made within QIA in terms of AFC fixed-delay multiplexed storage, both in time and frequency domain.

5.1. Time multiplexing in Europium doped Y_2SiO_5 (UNIGE)

UNIGE (in collaboration with ICFO) has worked on the theoretical temporal multimode capacity of AFC fixed-delay quantum memories, to better compare and quantify the multimode capacity [1]. The starting point of the theory is to fix a relation between the AFC bandwidth Γ and the modesize T . It can be shown that the Nyquist sampling theorem requires that $T > 2/\Gamma$, and by setting $T = 2.5/\Gamma$ one assures a high-fidelity storage of the temporal pulse train. For a storage time of $1/\Delta$, this result in a multimode capacity of

$$N_m = \frac{\Gamma}{2.5\Delta}. \quad (1)$$

Furthermore, it can be shown that for Gaussian input modes it is optimal to set $T = 2.38\tau$ in order to assure a good mode matching both in the time and frequency domain.

Experimentally UNIGE demonstrated storage of 100 temporal modes in a ^{151}Eu doped Y_2SiO_5 crystal, see Figure 1, where each temporal input mode contained about 1 photon in average (weak coherent states). The AFC memory scheme operated in its fixed-delay version, having a storage time of about $1/\Delta = 50 \mu\text{s}$. The AFC memory had a bandwidth of $\Gamma = 5 \text{ MHz}$, allowing storage of 100 temporal modes with a modesize of $T = 500 \text{ ns}$ and duration of $\tau = 210 \text{ ns}$ [1]. These settings were also found to be optimal experimentally.

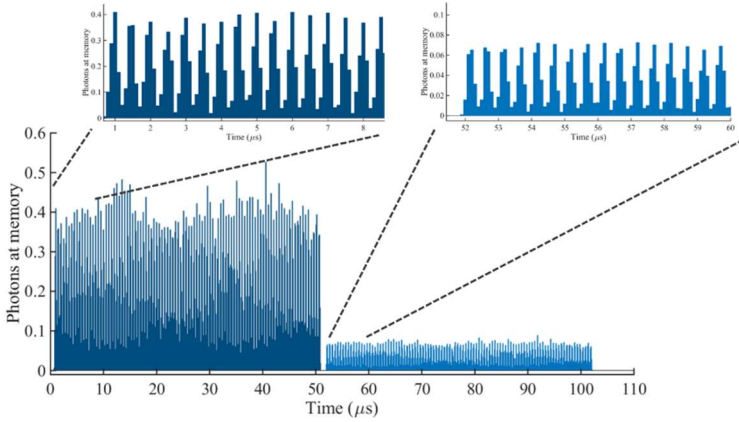
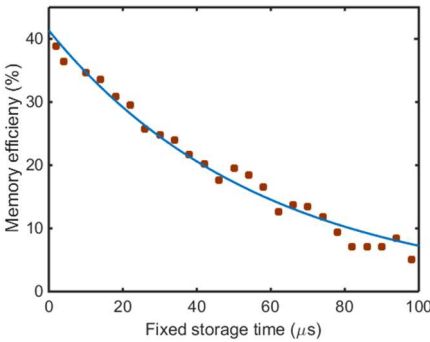


Figure 1: Storage of a train of 100 optical pulses, for a fixed duration of 50 μs . Vertical axis shows average number of photons at the memory. The integrated average number of pulses per pulse is about 1. The measured memory efficiency is 18%. The insets show the first 16 input and output pulses.

The UNIGE results were possible thanks to advances of the optimization of the AFC creation sequence, where a special sequence of optical pumping pulses is applied to the $^{151}\text{Eu}:\text{Y}_2\text{SiO}_5$ crystal. UNIGE performed numerical and experimental studies of how different parameters of the sequence affects the spectral resolution of the comb, and how the optical coherence time affects the memory efficiency. Progress were also made on the vibration-induced optical decoherence frequently observed in commercial closed-cycle cryogenic cooling systems. UNIGE has designed and tested several custom-made anti-vibration supports. The longest



measured fixed delay AFC memory storage time is shown in Figure 2, which currently is the state-of-the-art fixed delay storage time for any rare-earth-doped crystal. Yet, the long optical coherence time in this material should in principle allow 4 times longer decay time, and the current limitation is currently unknown.

Figure 2: AFC storage efficiency as a function of the fixed-delay storage time. The decay constant is $T_m = 58 \mu\text{s}$ (at the $\exp(-1)$ level). The short-delay efficiency of 41% is the highest reported for a AFC memory not based on cavity enhancement.

Figure 2 clearly shows that there is a inherent trade-off between the storage time $\frac{1}{\Delta}$ and memory efficiency. If we define a relative memory efficiency due to the efficiency decay time T_m as $\eta = \exp\left(-\frac{1}{\Delta T_m}\right)$, then one can express the multimode capacity in terms of the memory parameters Γ and T_m , for a fixed efficiency η : [1]

$$N_m = \frac{\ln(1/\eta)}{2.5} \Gamma T_m. \quad (2)$$

Note that T_m is fundamentally limited by $T_m = T_2/4$, where T_2 is the optical coherence time. The experiment shown in Figure 1 had a relative efficiency of $\eta = 0.42$, which resulted in 100 modes with $\Gamma = 5 \text{ MHz}$ and $T_m = 58 \mu\text{s}$, in agreement with eq. (2).

5.2. Time and frequency multiplexing in Praseodymium doped Y_2SiO_5 (ICFO)

ICFO demonstrated a spectrally (frequency) and temporally multiplexed solid-state quantum memory, based on the AFC scheme in a Praseodymium doped Y_2SiO_5 crystal waveguide [2]. Here the AFC scheme was operated in its fixed-delay version, with a storage

time of 3.5 μ s. They demonstrated quantum storage of the whole spectrum of a heralded single photon multiplexed along 15 discrete frequency modes separated by 260 MHz (spanning 4GHz). Thanks to the intrinsic temporal multimodality of the AFC scheme, each spectral bin includes 9 temporal modes, such that the total number of stored modes is about 135. It was demonstrated that the storage preserves the non-classical properties of the single photon, and its normalized frequency spectrum.

In the experiment, see Figure 3, 15 AFCs were created within the inhomogeneous broadening of the crystal, using electro-optic modulators (EOM) to create frequency sidebands for the preparation beam. They used a highly scalable method, in which, each EOM added to the setup, increases by a factor of three the number of frequency modes. In addition, the experiment was performed in an integrated waveguide, paving the way towards quantum memory arrays enabling high spatial multimodality. The multimode storage technique demonstrated in this paper is directly suitable for storing the frequency- bin entanglement naturally generated by the source. The stored excitation is heralded by a photon at telecom wavelength, making the protocol well suited for quantum repeater architectures [3, 4]. For that application each spectral channel is used as an independent quantum memory, leading to spectral multiplexing. This requires however the ability distinguish the different heralding frequency modes, i.e. to separate the different idler frequency modes. While this is challenging in the current experiment because the frequency separation is small, it may be achieved using e.g. virtually imaged phase arrays.

The number of stored modes can be strongly extended by increasing the storage time (for the temporal modes), generating bi-photons with over a larger frequency span and with smaller spacing between each spectral mode (for the frequency multiplexing), fabricating various waveguides throughout the crystal (for spatial-path multiplexing) or also extending to other degrees of freedom (for example orbital-angular momentum [5]).

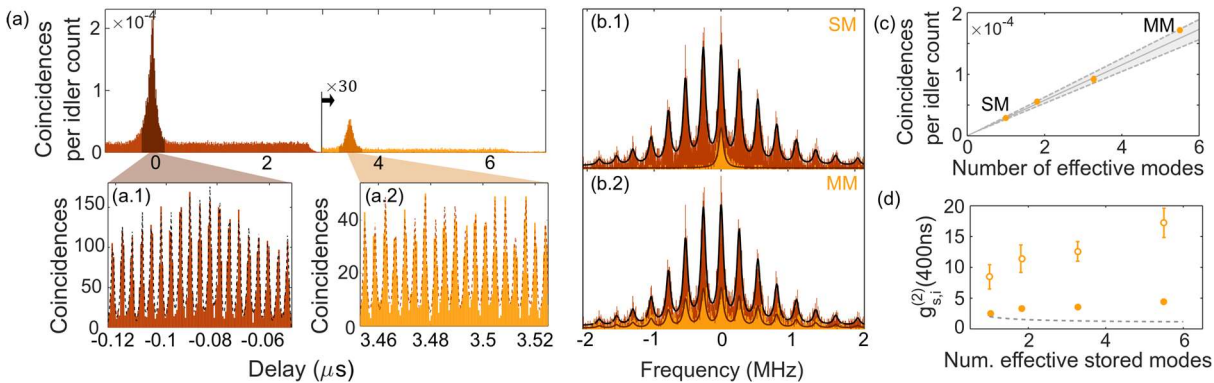


Figure 3: (a): Temporal coincidence histogram between idler and signal photons after the source (brown) or after storage (orange), with zoom of the coincidence peaks, (a.1) and (a.2), where the beating between the spectral modes is visible. (b.1) and (b.2): Heralded signal detections after a scanning filter cavity in the single-mode (SM) and multimode (MM) storage case, respectively. The brown (orange) histogram is measured with the source alone (after the storage). (c): Normalized coincidences between idler detections and signal photons after storage vs number of effective modes. The gray line is the expected behaviour extracted from the single-mode case. (d): Measured second-order cross correlation function $g_{s,i}^{(2)}$ vs number of effective modes stored. The orange full (empty) points are measured with $P = 3$ mW (1 mW). The gray dotted line is the theoretical classical limit, which scales with the number of modes N as $1 + 1/N$ (the real bound would be lower, due to noise and a finite detection window of 400 ns).

ICFO also demonstrated recently an entanglement experiment between two Pr:YSO crystals where single photons generated by cavity enhanced SPDC were stored in 62 temporal modes of 400 ns in fixed delay AFC memories with a storage time of 25 μ s [6]. Fig. 4a shows the decay of efficiency as a function of the storage time in the AFC, measured with single photons in the two Pr:YSO memories used for that experiment. The measured decay times are $T_m = 23$ μ s and $T_m = 14$ μ s (at the exp(-1) level) for the two memories. The difference between the two values is due to the fact that they have been measured in two different cryostats with different vibration isolation. The relative efficiency at 25 μ s is around 30 %. ICFO also demonstrated that the heralding rate of the entanglement between the two memories was enhanced by the multimode operation, while keeping the amount of entanglement

constant, see Figure 4b, in a scenario using a communication time of 25 μs , corresponding to a simulated distance of 5 km between the two quantum memories. This experiment highlights the advantage of using a multimode quantum memory for quantum repeater applications.

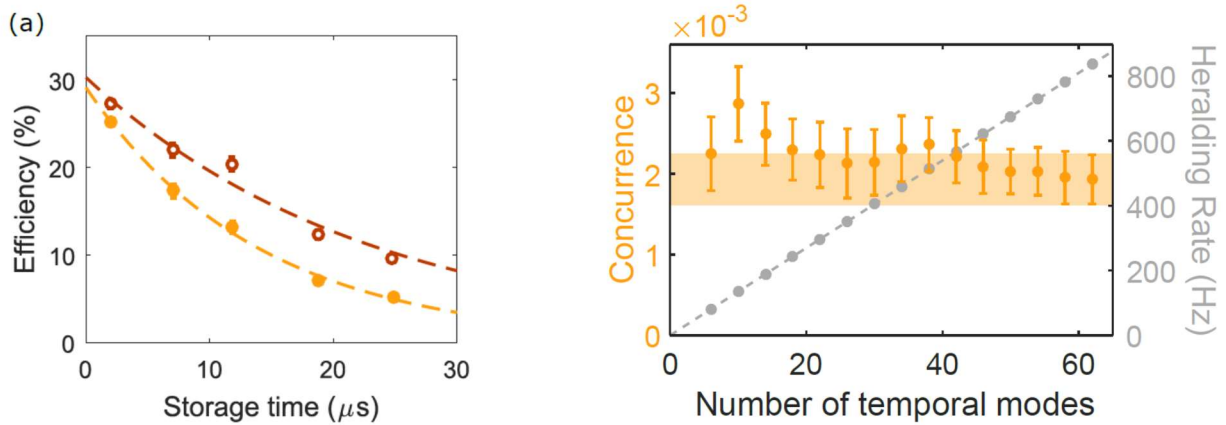


Figure 4: (a). Decay of AFC efficiency as a function of AFC storage time for two different Pr:YSO memories, measured with single photons. The measured decay times are $T_m = 23 \mu\text{s}$ and $T_m = 14 \mu\text{s}$ (at the $\exp(-1)$ level) for the two memories. (b) Advantage of using a temporally multimode quantum memory in a heralded entanglement experiment. The communication time considered is 25 μs , corresponding to a simulated distance between the memories of 5 km.

5.3. Frequency and time multiplexing in Tm:Y₃Ga₅O₁₂ (TUD)

TUD's work is based on thulium doped yttrium gallium garnet (Tm:Y₃Ga₅O₁₂, or Tm:YGG), a crystal whose promising spectroscopic properties the group has pointed out before [7], but whose potential for storing optical data had not yet been established. TUD now showed that the optical coherence time—a key property for achieving long optical storage times and hence a large temporal multimode capacity—can exceed 1 ms (see Fig 5a). This makes the transition almost radiatively limited and is the third-longest optical coherence time reported for any REIC. After having verified that the memory is suitable for quantum state storage, a measurement that relied on storing heralded single photons created using spontaneous parametric downconversion, the researchers also demonstrated storage times up to 100 μsec . This exceeds all previously obtained results with other rare-earth crystals except for what we report here for Eu:YSO (see Figure 1). These findings were obtained using laser pulses instead of quantum states of light. Similar to the results at UNIGE, TUD also found that the memory lifetime (the time after which the memory efficiency drops by $1/e$) is significantly shorter than what one would expect from the measurement of the optical coherence time. Possible reasons, which remain to be investigated, include vibrations of the crystal inside the pulse-tube cooler, remaining laser jitter, magnetic field instabilities, and spectral diffusion, e.g. due to gallium spin flips.

Due to the limited optical depth of the currently used crystal, all memory efficiencies were very small. However, simulations taking into account measured AFC profiles show that embedding the crystal into an impedance-matched cavity leads to very significant improvements, e.g. to around 63% at 10 μsec storage time, and 37% at 40 μsec . The experimental verification of these predictions is the topic of ongoing studies.

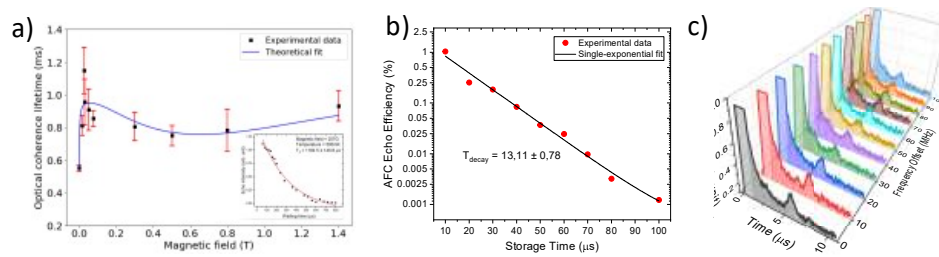


Figure 5: a) optical coherence time as a function of magnetic field, measured by means of 2-pulse photon echoes. The inset shows the decay of the photon-echo intensity as a function of waiting time between the first and second pulse for a magnetic field of 257 G. b) Memory efficiency and fitted decay. c) Spectro-temporal multiplexing, here with the example of 10 spectral modes and 5 μ sec storage.

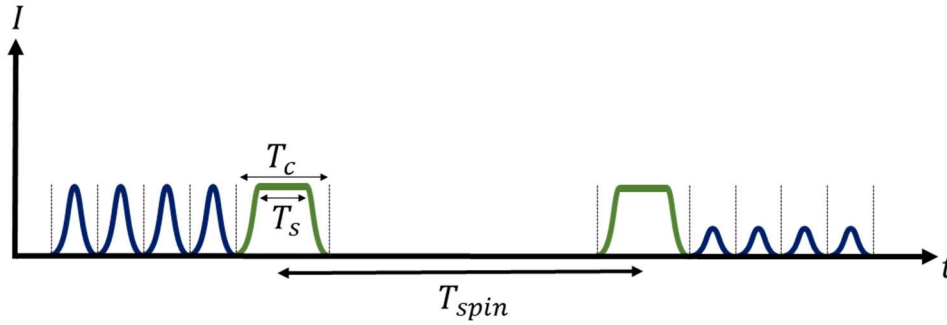
To demonstrate the spectral multiplexing capacity of our memory, TUD prepared 10 different AFCs, each of $\Gamma = 5$ MHz bandwidth and spaced by 25 MHz, over a total bandwidth of 250 MHz. 10 consecutive laser pulses of $\tau = 200$ nsec duration were created in each spectral mode, stored, and recalled after $1/\Delta = 5$ μ sec. Note that Eq. (1) also predicts a multimode capacity of 10 using these parameters. This resulted in a multi-mode capacity combined over the spectral and temporal degrees of freedom of 100. Fig. 5c shows the example of 11 spectral modes of 1 MHz width and optical pulses stored during 5 μ sec. Note that both the total bandwidth as well as the number of spectral channels can easily be increased with more laser power, which, given the inhomogeneous broadening of 56 GHz, would in principle allow creating thousands of spectral modes. At the same time, more laser power would also allow improving the AFC quality per spectral mode and thereby allow increasing the storage time by an order of magnitude and the multi-mode capacity by another factor of ten.

Finally, to meet the requirement of feed-forward-based mode mapping, imposed by the targeted use of a spectrally multiplexed memory in a quantum repeater, TUD furthermore demonstrated shifting of the recalled data pulses such that only the desired mode was subsequently transmitted through a filter cavity. For this proof-of-principle demonstration, laser pulses in three spectral modes were used, and each was stored during 20 μ sec.

A scientific document that details these investigations is under development.

6. Time multiplexing in solid-state quantum memories with on-demand read out

Long-duration and on-demand read out of AFC quantum memories can be achieved by reversible mapping of the optical coherence into a spin excitation, using two optical control pulse. We denote this memory as AFC spin-wave memory. The time sequence of input pulses, control pulses and output pulses are shown below (the control pulses are shown in green):



The main challenge of multimode AFC spin-wave storage is the low Rabi frequency on optical transitions, which generally require long control pulses to achieve efficient population inversion of the entire bandwidth Γ of the AFC. The duration of the control pulse will thus reduce the multimode capacity with respect to Eq. (2) for fixed-delay AFC memories. UNIGE has developed a theory for calculating the multimode capacity, by assuming that the control pulses are adiabatic HSH pulses. Using the notations as in Eqs. (1) and (2), the multimode capacity is [1]:

$$N_{m,sw} = \frac{\ln(1/\eta)}{2.5} \Gamma T_m - \chi \frac{4}{2.5\pi^2} \frac{\Gamma^2}{\Omega^2}. \quad (3)$$

where the additional parameters are the optical control pulse Rabi frequency Ω , and a HSH pulse shape parameter $\chi = T_c/T_s$ that is generally in the range of 1 to 2. The second term clearly shows the loss in multimode capacity due to the finite length of the control pulse, cf. Eq. (2) for optical fixed-delay AFC memories.

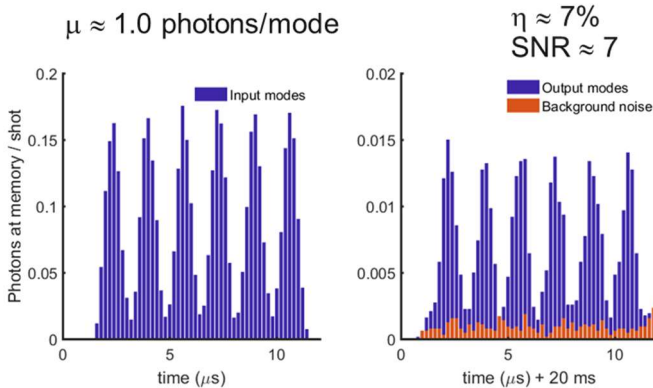


Figure 6: (left) Histogram of the 6 temporal input modes recorded with a transparent quantum memory for reference. Vertical axis shows average number of photons at the memory. The integrated average number of pulses per pulse is about 1. (right) The memory output modes are shown in blue, and the noise output, recorded without any input modes, is shown in red. The average efficiency is 7% and the average SNR is 7. The spin-wave storage time was 20 ms, the longest storage time in RE crystals at the single photon level.

Experimentally UNIGE has demonstrated storage of 6 temporal modes for a spin-storage duration of $T_{spin} = 20$ ms at the single photon level [8]. In Figure 6, we show an example of storage of weak coherent states of about 1 photon/mode at the input, with a SNR of 7 after 20 ms of storage.

In addition, storage of 2 time-bin qubit occupying 4 of the 6 modes showed a fidelity of 85% with an average photon number of about 1 in each qubit (i.e. 0.5 photons/mode in average).

The multimode capacity of the experiment shown above is mainly limited by the Rabi frequency Ω and the fact that, at the single photon level, the memory must be operated at a high relative efficiency of $\eta = 0.65$ to obtain a high SNR. In this experiment the relevant parameters where $\Gamma = 1.5$ Mhz, $T_m = 58$ μ s, $\Omega = 230$ kHz and $\chi = 1.38$, which gives indeed $N_{m,sw} = 6$ modes according to Eq. (3).

The limitations in current experiments in ^{151}Eu doped Y_2SiO_5 crystal are mainly due to the limited Rabi frequency and the optical memory decay time T_m . In Figure 7 (a) below we plot the theoretical multimode capacity for $\Gamma = 1.5$ Mhz and $\Omega = 230$ kHz as a function of T_m and relative efficiency of η , where the experiment shown above is shown as a white diamond. Clearly a significantly higher multimode capacity could be reached with a longer T_m . Note that the fundamental limit of $T_m > 250$ us in this material.

A second strategy is to increase the Rabi frequency, which can be achieved by using the strongest transition for the control field and the weaker one for the input modes, and to compensate the weaker absorption by using an optical cavity. In addition, by switching to ^{153}Eu doped Y_2SiO_5 the bandwidth can in principle reach $\Gamma = 15$ Mhz. By assuming a Rabi frequency of $\Omega = 1$ MHz, one could in principle reach a multimode capacity of 100 modes, as shown in Figure 7(b).

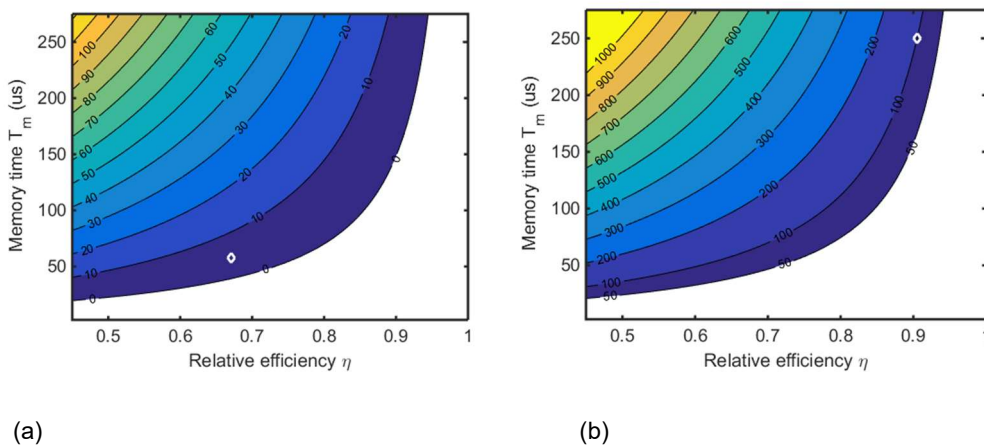


Figure 7: Contour plots of the AFC spin-wave temporal multimode capacity calculated with Eq. (3), as a function of relative optical memory efficiency η and the optical memory decay time T_m . In (a) the parameters where those describing current experiments in $^{151}\text{Eu}:\text{Y}_2\text{SiO}_5$, where the diamond corresponds to the experiment in Figure 6. In (b) we consider an optimized strategy with an increased Rabi frequency and a larger bandwidth in $^{153}\text{Eu}:\text{Y}_2\text{SiO}_5$, where one can potentially reach 100 modes and a very high relative efficiency of 90% simultaneously (see text for details).

ICFO also performed experiments demonstrating temporally multimode spin wave storage of single photon level pulses, in a Pr:YSO crystal [1]. Fig 8a shows the storage of 20 modes with on average 0.92 photon per pulse for a spin-storage duration of $T_{spin} = 14.2$ us. In this case, no dynamical decoupling is used such that the storage time in the spin state is limited by the spin-inhomogeneous broadening. A storage time in the AFC of 25 us was used, leading to an AFC efficiency $\eta_{AFC} = 7.7(3) \%$ and a relative efficiency of around $\eta = 0.3$. The spin wave storage and retrieval efficiency is 1.88 (3) % and the SNR of the retrieved pulses is 17.4 (4). The larger number of modes achieved compared to Eu:YSO is due in part to the fact that the Rabi frequency is larger the Pr:YSO crystal ($\Omega = 410$ kHz) and that a lower relative efficiency could be used to still achieve a good SNR, due to the lower noise floor in that experiment without dynamical decoupling. An experiment with storage of 30 modes was also performed (Fig 8b). In that case, the SNR (6.7 (1)) and spin wave efficiency (0.63 (1) %) were smaller because a longer spin-wave storage time (20.7 us) was used in order to avoid overlap between the retrieved spin wave modes and the AFC echoes.

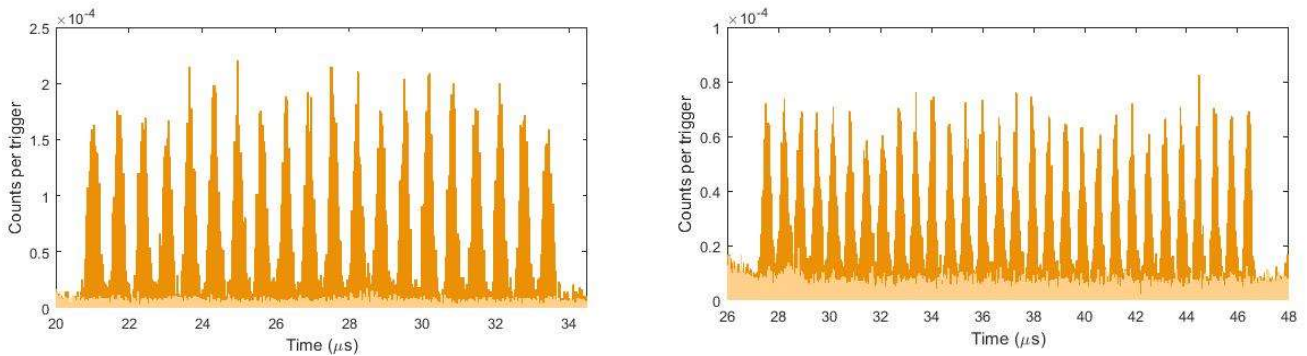


Figure 8: (a) Spin wave storage of 20 temporal modes in Pr:YSO (ICFO). The light orange curve represents the noise measured without input pulses. For this curve we have $SNR = 17.4(4)$ and $\eta_{SW} = 1.88(3) \%$. (b) Similar curve for 30 modes, with $SNR = 6.7(1)$ and $\eta_{SW} = 0.63(1) \%$. The lower efficiency and SNR are due to a longer spin-state storage time.

7. Space-division multiplexing in cold-atom-based quantum memories

SU has been working towards the demonstration of spatial division multiplexing (SDM) in cold-atom based quantum memories. This demonstration involves the setup of a photonic platform enabling multiplexing and demultiplexing of up to 15 spatial modes (Fig.1(a)), and the interfacing of this platform with the high-efficiency quantum memory SU previously developed as one milestone of QIA [8].

The photonic platform relies on a pair of mode-selective multiplexer-demultiplexer and associated optical components for addressing them. At the input, the apparatus acts as a multiplexer and converts the output of 15 independent single-mode fibers into a single collimated beam made of 15 orthogonal Hermite-Gaussian modes. The single beam is then collected by an identical apparatus acting as a demultiplexer and converting, in turn, the composite beam back to the original collection of 15 independent beams. SU has incorporated this system in their quantum memory experiment and connected it with their D1-line laser system (Fig.1(b)). This

is done using a “polarization tree” which splits an input beam coming from the D1-line laser system into 15 beams. Each one of these beams is then coupled to a polarization maintaining single-mode fiber which connects to each channel of the multiplexing platform via a fiber-to-fiber connection board (Fig.1(c)).

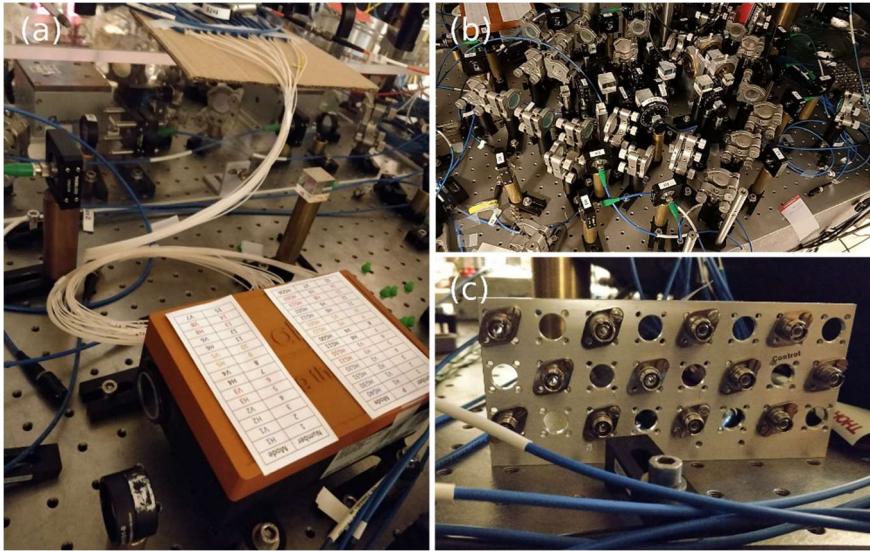


Figure 9: The multiplexing-demultiplexing system incorporated to the quantum memory experiment. (a) Photonic platform here acting as a demultiplexer with its collimating lens at the input and 15 single-mode polarization maintaining fibers at the output. (b) The “polarization tree” splitting an input D1-line beam into 15 independent beams used for multiplexing. (c) The fiber-to-fiber connection board allowing to link the polarization tree to the multiplexer.

SU has fully characterized the photonic platform after its integration to the existing experimental system. The response in transmission of both the multiplexing and demultiplexing devices has been evaluated and the overall efficiency of the multiplexing-demultiplexing procedure, for each mode, without the presence of cold atoms, has also been evaluated. These measurements allowed to establish the transfer matrix of the system and assess the degree of cross-talk for each multiplexing channel. The transfer matrix is presented in Fig.2.

(dB)		Output														
		HG00	HG10	HG01	HG20	HG11	HG02	HG30	HG21	HG12	HG03	HG40	HG04	HG22	HG31	HG13
Input	HG00															
	HG10	-37.5														
	HG01	-37.6	-22.9													
	HG20	-22.6	-21.2	-21.5												
	HG11	-37.4	-38.8	-36.3	-25.1											
	HG02	-37.5	-39	-21.5	-30.5	-23.5										
	HG30	-26	-23.5	-25.7	-22	-29.2	-38.7									
	HG21	-37.3	-38.8	-24.9	-20.1	-19.6	-37.9	-30.2								
	HG12	-38.1	-20.5	-37	-39.1	-24.1	-24.8	-22.3	-32.7							
	HG03	-25.6	-25.9	-19.7	-38.7	-23.7	-17.6	-30.6	-34.8	-35						
	HG40	-25.5	-18.2	-36.5	-18.1	-28.6	-28.7	-15.3	-34.7	-34.9	-28					
	HG04	-37.6	-25.9	-21.6	-21.5	-37.3	-24.4	-37.3	-32.3	-28.6	-13	-26.2				
	HG22	-22.9	-23.3	-36.9	-23.3	-28.9	-22.5	-24.6	-22.7	-35.3	-23.7	-26.5	-36.4			
	HG31	-37.8	-39.2	-36.7	-23.2	-21.5	-38.4	-16	-19.8	-28.7	-23.5	-37.6	-36.2	-29.8		
	HG13	-37.9	-23.2	-25.5	-23.2	-21.6	-24.6	-24.5	-35	-17.8	-15.6	-37.7	-19.9	-15.3	-27.4	

Figure 10: Full transfer matrix of the system showing cross-talks >-20 dB for each modal channel.

The next stage, i.e. the mapping of the 15 spatial modes into the quantum memory, has been delayed due to the lab-access restrictions imposed during the Covid-19 pandemic. Since March 2020, the lab access has been limited on average to 50% of its nominal capacity, and limited to 20% during the two lockdowns. The restrictions applied to PhD students and postdoctoral researchers alike.

During this time, SU carried out numerical simulations to assess the modal capacity of their quantum memory and compute the expected mapping fidelity of each mode. Those simulations are based on methods developed by the group of A. Sørensen with Bessel modes [9] and preliminary results give a capacity estimate of the order of 100 spatial modes.

The milestone has therefore been delayed and should be postponed to the end of the project. Prior to storing spatially-multiplexed photons in the quantum regime, SU will first run the experiment using attenuated coherent beams in each mode and store them in the memory using EIT. This will establish an empirical characterization of the setup and should allow SU to study the influence of the number of modes on the memory efficiency and associated cross-talks.

The number of spatial modes that can be multiplexed in SU current setup is limited to 15. However, the company Cailabs has recently developed an upgraded version of their device allowing up to 45 modes to be multiplexed-demultiplexed in wavelengths compatible with Cesium transitions.

8. Conclusion

In this report we have presented temporal and frequency multiplexing of more than 100 modes in solid-state quantum memories, using fixed-delay AFC quantum memories. These results fulfill MS20, and they were obtained in the groups at UNIGE, ICFO and TUD. A theory allowing for quantitative analysis of the temporal multimode capacity was also developed, given experimental parameters for each platform. In terms of multi-mode storage using on-demand spin-wave AFC memories, multimode capacities up to 30 modes were demonstrated using only temporal multiplexing. The limitation of the current spin-wave memory temporal capacity was carefully analysed, showing that there exist a realistic strategy that should allow up to 100 modes to be stored. In addition, the overall capacity can also be increased using frequency multiplexing, as for the fixed-delay memory experiments.

Spatial multiplexing for cold-atom quantum memories was also investigated by SU, however, due to severe Covid-19 related restrictions it has not been possible to perform a spatial multiplexing storage experiment at SU. Nevertheless, SU has fully characterized the transfer matrix of the photonic platform that will allow storage of 15 spatial modes, demonstrating low cross talk between spatial modes (>-20 dB). SU now plans to store attenuated coherent beams in each mode, with the EIT memory scheme. A theoretical analysis show that potentially up to 100 modes could be stored in the future, and it is anticipated that the platform manufacturer will soon be able to provide a practical device allowing up to 45 modes.

9. References

- [1] A. Ortu, A. Holzäpfel, J. Rakonjac, A. Seri, H. de Riedmatten and M. Afzelius, *article manuscript under preparation*
- [2] A. Seri, D. Lago-Rivera, A. Lenhard, G. Corrielli, R. Osellame, M. Mazzer, and H. de Riedmatten, Phys. Rev. Lett. 123, 080502 (2019)
- [3] C. Simon, H. de Riedmatten, M. Afzelius, N. Sangouard, H. Zbinden, and N. Gisin, Phys. Rev. Lett. 98, 190503 (2007)
- [4] N. Sinclair, E. Saglamyurek, H. Mallahzadeh, J. A. Slater, M. George, R. Ricken, M. P. Hedges, D. Oblak, C. Simon, W. Sohler, and W. Tittel, Phys. Rev. Lett. 113, 053603 (2014)
- [5] T. Yang, Z. Zhou, Y. Hua, X. Liu, Z. Li, P. Li, Y. Ma, C. Liu, P. Liang, X. Li, Y. Xiao, J. Hu, C. Li, and G. Guo, Nature Comm. 9, 3407 (2018)
- [6] D. Lago-Rivera, S. Grandi, J. V. Rakonjac, A. Seri, and H. de Riedmatten, arXiv:2101.05097 (to appear in Nature)
- [7] C. W. Thiel, N. Sinclair, W. Tittel, and R. L. Cone, Phys. Rev. Lett. 113, 160501 (2014).
- [8] A. Ortu, A. Holzäpfel, and M. Afzelius, *article manuscript under preparation*
- [8] M. Cao, F. Hoffet, S. Qiu, A. S. Sheremet, J. Laurat, Optica 7, 1440 (2020)
- [9] A. Grodecka-Grad, E. Zeuthen, A. S. Sørensen, Phys. Rev. Lett. 109, 133601 (2012)